

Mechanical Manipulations on Electronic Transport of Graphene Nanoribbons

Jing Wang¹, Guiping Zhang^{1,*}, Fei Ye², and Xiaoqun Wang^{1,3,4,5†}

¹*Department of Physics, Renmin University of China, Beijing 100872, China*

²*Department of Physics, South University of Science and Technology of China, Shenzhen 518055, China*

³*Beijing Laboratory of Optoelectronics Functional Materials and Micronano Device, Renmin University of China, Beijing 100872, China*

⁴*Department of Physics and Astronomy, Shanghai Jiao Tong University, Shanghai 200240, China and*

⁵*Collaborative Innovation Center of Advanced Microstructures, Nanjing 210093, China*

(Dated: May 13, 2015)

We study the effects of uniaxial strains on the transport properties of the graphene nanoribbons (GNRs) connected with two metallic leads in heterojunctions, using the transfer matrix method. Two typical GNRs with zigzag and armchair boundaries are considered, and the tension is applied either parallel or perpendicular to the ribbon axis. It turns out that the electron-hole symmetry is missing in the gate voltage dependence of the conductance data of the armchair GNRs, while it persists in the zigzag ribbons under any strains. For an armchair GNR with a vertical tension applied, a sharp drop of conductance is found near the critical value of the strain inducing a quantum phase transition, which allows to determine the critical strain accurately via measuring the conductance. In the zigzag ribbon, there exists a range of gate voltage around zero, where the conductance is insensitive to the small horizontal strains. The band structures and low-energy properties are calculated to elucidate the mechanism on the strain effects in GNRs. We expect that our results can be useful in developing graphene-based strain sensors.

PACS numbers: 72.80.Vp; 73.22.Pr; 74.25.F-; 73.40.Sx

I. INTRODUCTION

Graphene has attracted widespread interests both theoretically and experimentally since its discovery in 2004, because of its unique properties and promising applications[1–3]. Recently, there are many studies on its mechanical deformation[4, 5] and the corresponding effects on the Raman spectroscopy[6], since the strain is inevitable for the fabrication of graphene on substrate. Unlike the conventional materials, graphene has a tough mechanical property and could sustain elastic deformation up to $15 \sim 20\%$ [7, 8]. There are two typical ways to control the strain in graphene samples[6, 7]. One way is using the substrate with an array of holes with diameter ranging from $1\mu\text{m}$ to $1.5\mu\text{m}$. When a free-standing monolayer graphene is transferred onto it, a nonlinear strain-stress relation is observed by nanoindentation in the atomic force microscope[7], which has been verified theoretically[8]. The other one is by exerting tension on the substrate to control the strain on the graphene[6, 9, 10]. Graphene ripples on polydimethylsiloxane (PDMS) substrate can afford a reversible structural deformation under tensile strains as large as $20 \sim 30\%$ [11].

At atomic scale, the C-C bond length is changed by the strain, so are the hopping integrals and the band structure of graphene. To open a band gap in graphene, one requires a uniaxial strain in excess of 20% , which is beyond the range of elastic deformation[12].

In contrast, a much smaller uniaxial strain can control (close or open) the band gap in the narrow armchair graphene nanoribbons (AGNRs), while the zigzag graphene nanoribbons (ZGNRs) are quite robust against gap opening for small strain [13–15].

In recent years, the field of graphene-based strain sensors develops rapidly, since it is feasible to mediate electronic properties of graphene by applying tensions. In a sample of graphene from chemical vapor deposition, the resistance remains around $7.5K\Omega$ under the strain less than 2.47% applied along the electronic transport direction, while increases rapidly to $25K\Omega$ under 5% strain[9]. This is because that the ripples in graphene do not disappear until the strain exceeds 2.47% . The strain dependent transport properties enable graphene to have potential applications in the fields of the displays, robotics, fatigue detection, body monitoring, and so forth. For instance, the graphene-based strain sensors on the transparent gloves can measure the magnitudes and directions of the principal strains on the glove induced by the motion of fingers[10].

The previous theoretical investigations on the transport properties of the strained graphene nanoribbons[16–22] mostly deal with the small-scale GNRs with a width of about several nanometers using homojunction contacts, while one may encounter more complicated situations in practice, e.g., heterojunction contacts and wider GNRs in the fabrication of the GNR-based nanodevices. In this paper, we utilize a transfer matrix method[23] to study the transport properties of both narrow and wide GNRs under the strain, which are in particular connected to two metallic leads with heterojunctions. The width of graphene can reach the order of microns by means of the transfer matrix method[23]. A tight binding model is

*Electronic address: bugubird'zhang@hotmail.com

†Electronic address: xiaoqunwang@ruc.edu.cn

taken to describe the low energy physics for both the π -electrons of graphene and metallic electrons in two leads. The effects of strains on the hopping integral of C-C bonds in graphene are elucidated in Sec.II. The band structures of AGNRs and ZGNRs for various sizes under different strains are presented in Sec.III. In Sec. IV, we show the effects of strains on the transport properties of both AGNRs and ZGNRs. The edge effects are discussed in Sec. V. We note that strain only affects the band structure of graphene and the electronic transport of strained graphene we present embodies the combined effects of strains and the heterojunctions composed of graphene and metallic contacts.

II. MODEL AND METHOD

A. Strained Graphenes

To investigate the influence of uniaxial strain on the electronic transport properties of GNRs, we connect it with semi-infinite quantum wires, which are characterized by the square lattices, as illustrated in Fig. 1. Each interface between the GNR and a lead is a heterojunction. For AGNRs in Fig. 1(a), the interface is a ring consisting of five atoms, which eventually breaks the electron-hole(e-h) symmetry of the system, while for ZGNRs in Fig. 1(b), each ring at two interfaces contains four or six atoms which retains the e-h symmetry since the tight binding model involves only the nearest neighbor hopping in this paper. This is revealed by the dependence of conductance on gate voltages as shown later. The uniaxial tension is only applied to the GNRs leading to the deformation of C-C bonds in an anisotropic way.

The strain-stress relation for graphene is given in Ref. [12]. We quote those relevant results here for our further discussions. The tension is applied along the direction $\cos\theta\vec{e}_x + \sin\theta\vec{e}_y$, and the corresponding tensile strains parallel and perpendicular to this direction are S and $-\nu S$, respectively, with the Poisson's ratio $\nu = 0.165$ [24]. In the lattice coordinate system the strain tensor reads

$$\epsilon = S \begin{pmatrix} \cos^2\theta - \nu\sin^2\theta & (1+\nu)\cos\theta\sin\theta \\ (1+\nu)\cos\theta\sin\theta & \sin^2\theta - \nu\cos^2\theta \end{pmatrix}. \quad (1)$$

For any vector \vec{l}_0 in the undeformed graphene plane, it is straightforward to obtain its deformed counterpart to the leading order by the transformation

$$\vec{l} = (1 + \epsilon)\vec{l}_0. \quad (2)$$

The hopping amplitude t_i with $i = 1, 2, 3$ as defined in Fig. 1 is determined by the corresponding bond length δ_i via the following formula[12]

$$t_i = t_0 e^{-3.37(\frac{\delta_i}{a}-1)}, \quad (3)$$

with $t_0 = 2.6\text{eV}$ and $a = 1.42\text{\AA}$ for the undeformed graphene. The bond length δ_i under the strain can be

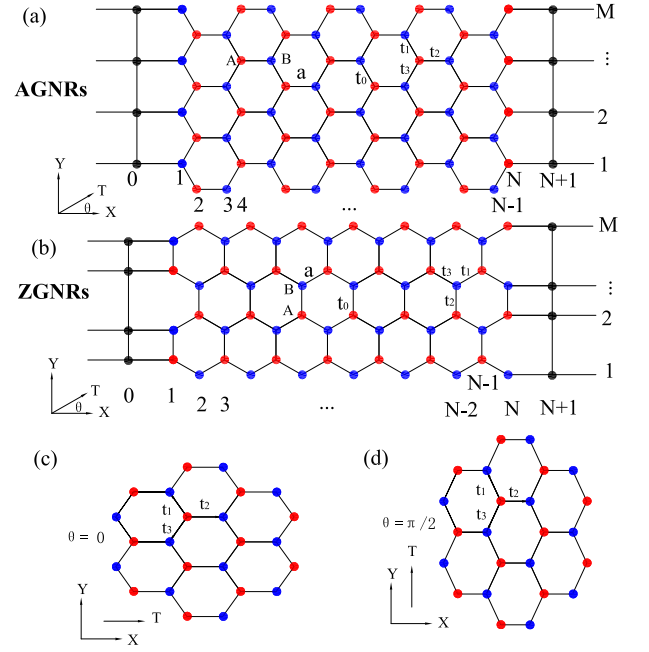


FIG. 1: (Color online.) The schematic illustration of AGNRs (a) and ZGNRs (b), connected to two semi-infinite quantum wires. There are N and M carbon atoms in x and y directions, respectively. (c) AGNRs with the tension along x -axis, i.e. $\theta = 0$, and (d) along y -axis with $\theta = \pi/2$.

calculated by Eq. (1) and Eq. (2). Without loss of generality, we focus on two cases with $\theta = 0$ and $\pi/2$ as follows.

- For $\theta = 0$ shown in Fig. 1(c),

$$\delta_1 = \delta_3 = (1 + \frac{1}{4}S - \frac{3}{4}\nu S)a, \quad \delta_2 = (1 + S)a.$$

All the three bond lengths increase as S increases, and the t_i 's subsequently decrease for all $i = 1, 2, 3$. However, δ_2 increases faster than δ_1 and δ_3 . Therefore, we have $t_1 = t_3 > t_2$ as long as $S > 0$.

- For $\theta = \pi/2$ shown in Fig. 1(d),

$$\delta_1 = \delta_3 = (1 + \frac{3}{4}S - \frac{1}{4}\nu S)a, \quad \delta_2 = (1 - \nu S)a.$$

In this case, we also have $\delta_1 = \delta_3$ and $t_1 = t_3$. As S increases, $\delta_{1,3}$ increase, while δ_2 decreases. It turns out that t_1 and t_3 decrease and t_2 increases with increasing $S > 0$.

For ZGNRs, the lattice coordinate system is rotated by $\pi/2$ from that of AGNRs. Therefore, the strain effect on the hopping amplitudes for ZGNRs with $\theta = 0$ (or $\pi/2$) is identical to that for AGNRs with $\theta = \pi/2$ (or 0). The hopping amplitudes t_i 's as functions of S are plotted for AGNRs in Fig. 2(a), in the unit of t_0 , which is set as one in the following discussions.

B. Tight-binding Model and Transfer Matrix Method

The π -electrons of carbon atoms are responsible for the low energy physics of graphene which can be described by the tight binding model on the honeycomb lattice

$$\hat{H} = \sum_{\langle ij, i'j' \rangle} t_{ij, i'j'} \hat{c}_{ij}^\dagger \hat{c}_{i'j'} + V_g \sum_{ij} \hat{c}_{ij}^\dagger \hat{c}_{ij}, \quad (4)$$

where a pair of integers ij indicates the lattice position $\vec{R}_{ij} = x_i \vec{e}_x + y_j \vec{e}_y$, and \hat{c}_{ij} (\hat{c}_{ij}^\dagger) is the corresponding electron annihilation (creation) operator. The summation is over the nearest neighbors indicated by $\langle \dots \rangle$, and $t_{ij, i'j'}$ is the hopping amplitude which takes the value of t_1 , t_2 or t_3 depending on the relative position $\vec{R}_{i'j'} - \vec{R}_{ij}$. The spin indices of electrons are omitted simply for convenience. V_g is the gate voltage which is applied only to the GNRs, not on the leads. In our simulation, we consider a simplified case with V_g changing abruptly at the interfaces between the GNR and the leads. In fact, this simplification is reasonable for small V_g . For large V_g , there may exist a junction between the leads and GNR with finite width of several atoms. This situation would not be considered here, since it only incurs further unnecessary complexities as far as the strain effects are concerned.

The left and right electrodes are also described by the Hamiltonian in Eq. (4) with $V_g = 0$, but the lattice vectors \vec{R}_{ij} describe a rectangular lattice instead of the hexagonal one. All the hopping integrals in the leads are fixed as t_0 , despite the vertical lattice constants may not be uniform in the leads connected to ZGNRs as shown in Fig. 1b. We also assume the leads are unaffected by the strain in our numerical simulation. This idealized setup mimics a normal-metal/GNR heterojunction, by which we shall demonstrate the strain effects on the transport through GNRs.

The single-particle eigenstate with energy E can be expressed as $\hat{\psi}^\dagger(E) = \sum_{ij} \alpha_{ij} \hat{c}_{ij}^\dagger$, which satisfies $[\hat{\psi}(E), \hat{H}] = E \hat{\psi}(E)$, leading to

$$(E - V_g) \alpha_{ij} = \sum_{\langle ij, i'j' \rangle} t_{ij, i'j'} \alpha_{i'j'}. \quad (5)$$

The wavefunctions of the electrodes can be represented in terms of two numbers k_x and k_y , where k_x describes the plane wave traveling along the x direction and k_y is quantized as $k_{y,n} = n\pi/(M+1)$ with $n = 1, 2, \dots, M$ due to the open boundary condition imposed in the y direction, to characterize different channels. The corresponding eigenenergy reads

$$E = 2t_0(\cos k_{y,n} + \cos k_{x,n}), \quad (6)$$

which determines the wave number $k_{x,n}$ in n -th channel for the given Fermi energy E . Note that, since the hopping amplitudes of all the bonds are given, the lattice

constant is not needed anymore and one can simply use dimensionless wave numbers $k_{x,n}$ and $k_{y,n}$ to label the quantum states.

If we assume the electrons are incident from the left, the wavefunctions in the left and right electrodes can be written as [23, 25]

$$\begin{aligned} \alpha_{ij}^L &= \sum_{n'} (\delta_{n'n} e^{ik_{x,n'} x_i} + r_{n'n} e^{-ik_{x,n'} x_i}) \sin(k_{y,n'} y_j), \\ \alpha_{ij}^R &= \sum_{n'} t_{n'n} e^{ik_{x,n'} x_i} \sin(k_{y,n'} y_j), \end{aligned} \quad (7)$$

where $t_{n'n}$ and $r_{n'n}$ are the transmission and reflection amplitudes from n -th to n' -th channel, respectively. Current conservation requires $\sum_{n'} \eta_{n,n'} [|t_{n,n'}|^2 + |r_{n,n'}|^2] = 1$ for each n with $\eta_{n,n'} \equiv |\sin(k_{x,n'})|/|\sin(k_{x,n})|$. In order to calculate the transmission coefficients $t_{n,n'}$, we adopt the transfer matrix method developed in Ref. 23, and then we can designate α_j for the M coefficients with column index j , which satisfies the matrix equation

$$\begin{pmatrix} \alpha_j \\ \alpha_{j+1} \end{pmatrix} = \chi_j \begin{pmatrix} \alpha_{j-1} \\ \alpha_j \end{pmatrix}, \quad (8)$$

where χ_j is the $2M \times 2M$ transfer matrix as a function of Fermi energy E , gate voltage V_g and the hopping amplitudes t_i 's. By acting the transfer matrices consecutively, the coefficients in the left and right interfaces are connected in the following form

$$\begin{pmatrix} \alpha_N \\ \alpha_{N+1} \end{pmatrix} = \chi_N \chi_{N-1} \dots \chi_2 \chi_1 \begin{pmatrix} \alpha_0 \\ \alpha_1 \end{pmatrix}. \quad (9)$$

Combining Eq. (7) and Eq. (9) one can obtain the transmission and reflection coefficients $t_{n,n'}$ and $r_{n,n'}$. In order to investigate the transport properties of the large scale GNRs, we actually utilize the renormalized transfer matrix method as described in Ref. 26. It is straightforward to calculate the conductance by employing Landauer-Büttiker formula

$$G = \frac{2e^2}{h} \sum_{n,n'=1}^M \eta_{n,n'} |t_{n,n'}|^2, \quad (10)$$

where the factor 2 is a consequence of the spin degeneracy.

III. BAND STRUCTURE OF STRAINED GRAPHENE NANORIBBONS

In this section, we study the band structure and low energy excitations of GNRs under strains by solving the tight binding model Eq. (4) with the hopping amplitudes given by Eq. (3). For convenience, we impose the periodic boundary condition along x -axis and the open boundary condition along y -axis, and the energy E is taken in unit of t_0 in the following discussions. We also assume the horizontal lattice spacing to be unit so that k_x is always in the interval $[0, 2\pi)$, although it changes as the tension is applied.

A. Strained AGNRs

The spectra of AGNRs are plotted in Figs. 2(b)-(f) as functions of k_x with $N = 100$ and $M = 100$ for different strains. The unstrained data is given in Fig. 2(b) which is precisely gapless at $k_x = 0$. In the presence of strains, the spectrum changes upon the direction of the applied tension. When the tension is applied horizontally to AGNRs, i.e. $\theta = 0$, the spectra in Figs. 2(c) and (e) are similar to the unstrained case, except that the uniaxial strain may open a small gap at $k_x = 0$. This gap is proportional to M^{-1} and becomes almost invisible for $M = 100$, which results from the combined effect of the finite ribbon widths and the strains. When the tension is applied vertically, i.e. $\theta = \pi/2$, the spectrum in Fig. 2(d) with strain $S = 0.15$ shows a tiny gap, which is also proportional to M^{-1} with the same origin of that for $\theta = 0$. For $S = 0.3$, another type of gap opens at $k_x = 0$ as shown in Fig. 2(f), which is induced entirely by the strain [12] and can survive the thermodynamic limit unlike the previous gaps. In fact there is a critical strain S separating the two different gaps as to be discussed in details later.

Figures 2(g) and (h) show the density of states (DOS) $\rho(E)$ for AGNRs under different strains for $\theta = 0$ and $\pi/2$, respectively. The band width is $D = 2t_1 + t_2$ plus a negligible dependence on the ribbon width, which obviously shrinks as S increases for both $\theta = 0$ and $\theta = \pi/2$, although t_1 ($t_3 = t_1$) and t_2 behave very differently as functions of S in Fig. 2(a). When $\theta = 0$, t_1 and t_2 are decreasing function of S so is the band width. When the strain increases for $\theta = \pi/2$, t_2 increases, but it is the decreasing t_1 that dominates the strain dependence of the band width. Besides the shrinking band width, there are no other common features in the DOS for both cases with $\theta = 0$ and $\theta = \pi/2$. For the unstrained ribbons, there are two peaks of DOS located at $\pm t_0$. Each of them splits into double peaks if the tension is applied horizontally, which locate at $\pm t_2$ and $\pm(2t_1 - t_2)$ as seen in Fig. 2(g). When the tension is applied vertically, the peaks at $E = \pm t_2$ in Fig. 2(h) move slightly outwards instead of splitting. However no peaks are observed at $E = \pm(2t_1 - t_2)$, except two shoulders emerging at $\pm 0.5t_0$ for $S = 0.1$ as a remnant of the peaks. For other strains in Fig. 2(h), even the shoulders can not be seen. When the strain $S = 0.3$, the DOS vanishes in the energy range $[-0.205, 0.205]$ implying a gap of $0.409(t_0)$ opens.

Now we turn to the dependence of energy gaps at $k_x = 0$ on the ribbon widths and strains. For the unstrained AGNRs, the gap is zero for $\text{mod}(M, 3) = 1$ and inversely proportional to M for $\text{mod}(M, 3) = 0, 2$, which coincides with previous studies using the first-principle calculation [27] and the tight binding model [23, 28]. This feature is manifested in Figs. 3(a)-(d) for $M = 10, 11, 12, 49$ and 100 with a fixed ribbon length $N = 100$.

When the tension is applied horizontally with different ribbon widths, the band gaps oscillate with the strains in the similar zigzag patterns, but with different “phases”

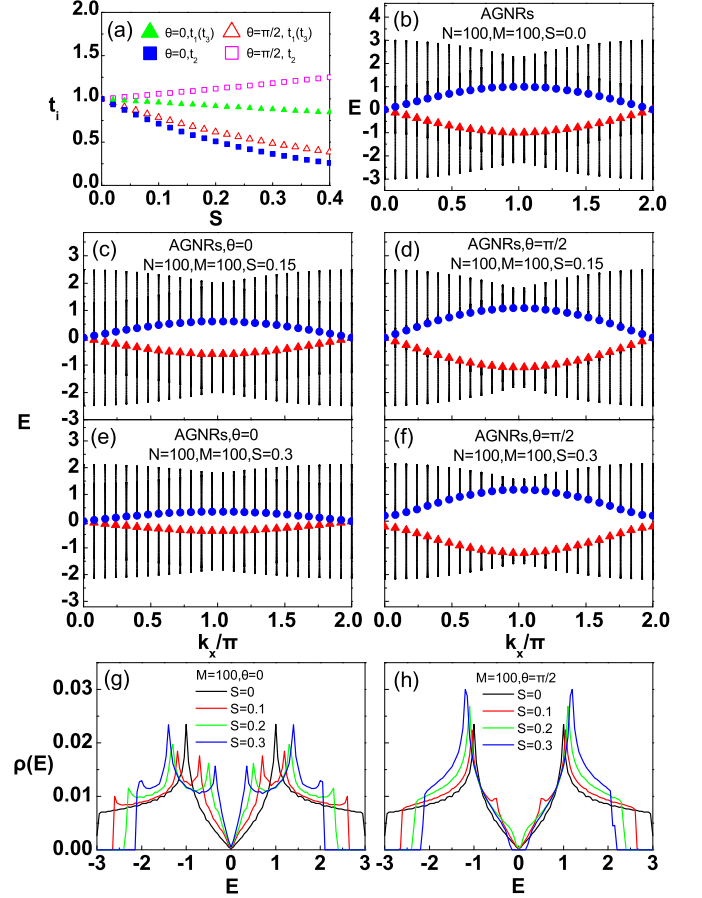


FIG. 2: (Color online.) (a) shows the strain dependence of the three hopping amplitudes. (b)-(f) are the band structures of AGNRs with $N = M = 100$ under various strains. (g) and (h) are the density of states $\rho(E)$ of AGNRs with $M = 100$ and $N = 1600$ for the tensions along x and y axis, respectively.

according to different values of $\text{mod}(M, 3)$ as shown in Fig. 3(a). The oscillatory amplitude is inversely proportional to M and barely changes with S , and the oscillatory frequency increases with M , but decreases with S as shown in Fig. 3(c).

For $\theta = \pi/2$ as shown in Figs. 3(b) and (d), the band gap behaves significantly different from that for $\theta = 0$. The oscillation only happens for $S < S_c$. In this region, the oscillatory amplitude decreases with both M and S , while the frequency increases with both M and S . The band gaps for both $\theta = 0$ and $\theta = \pi/2$ result from the combined effects of the strains and the finite ribbon widths. Actually they are almost invisible in Fig. 3(e) for M as large as 1000. The essential difference occurs for $S > S_c$, where a gap opens for $\theta = \pi/2$ with a dominant linear dependence on $S - S_c$ in the thermodynamic limit. This is demonstrated with the finite- M scaling for different values of S in Fig. 3(f).

In fact, for AGNRs with vertical strains, the gap opening implies a quantum phase transition occurring at $S = S_c$ from a Fermi liquid to a dimerized solid phase.

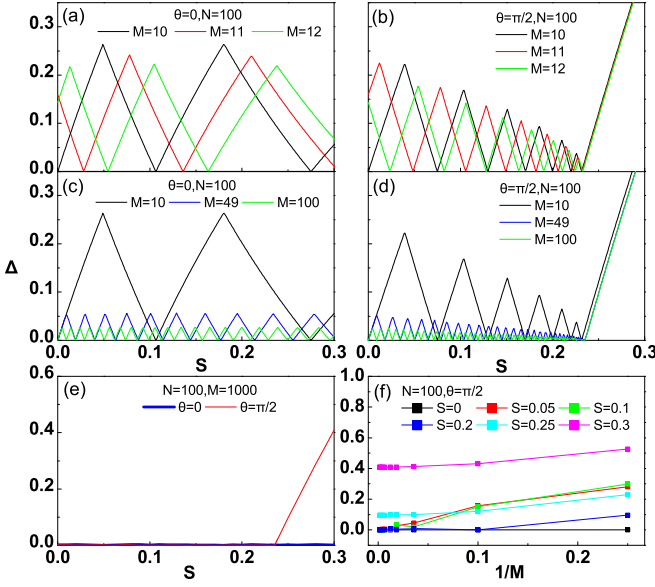


FIG. 3: (Color online) Band gaps of AGNRs as functions of strains with various sizes. The tension is applied horizontally in (a) and (c), and vertically in (b) and (d). A very large ribbon width $M = 1000$ is taken in (e) for both $\theta = 0$ and $\pi/2$, where the finite size effect is too small to be observable. (f) shows the extrapolation of the band gap to the infinite width limit under various strains in the case of $\theta = \pi/2$.

As shown in Fig. 2(a), t_2 increases and $t_{1,3}$ decrease with increasing S for $\theta = \pi/2$, which eventually leads to the dimerized t_2 -bonds with an energy gap $\Delta = 2|t_2 - 2t_1|$ opening. The critical strain $S_c = 0.235$ can be determined by solving the equation $\Delta(S) = 0$, or equivalently $t_2(S) = 2t_1(S)$ [12]. It is then understandable that the gaps of AGNRs with finite widths diminish to zero as S approaching S_c from the left, since a quantum phase transition occurs there. For $\theta = 0$, all t_i 's decrease with S monotonically, and t_2 decreases even faster, hence there is no phase transition at all.

B. Strained ZGNRs

In this subsection, we discuss the band structure of ZGNRs with the periodical boundary condition in x direction and open boundary condition in the y direction. Fig. 4(a) is the band structure of unstrained ZGNRs, which shows a midgap flat band corresponding to the edge states[29] localized in the upper and lower zigzag boundaries. The flat band exists in a finite region of momentum $[k_s, 2\pi - k_s]$ with $k_s = 2\pi/3$ for the unstrained ribbon determined by the convergent condition for the wavefunction of the edge states $|2\cos(k_x/2)| \leq 1$ [29].

When the tension is applied, apart from those effects on the valence and conduction bands, the region of the momentum for the flat band is also affected by strain as seen in Fig. 4. For the horizontal strain of $\theta = 0$ as shown in Figs. 4(c) and (e), k_s moves towards zero

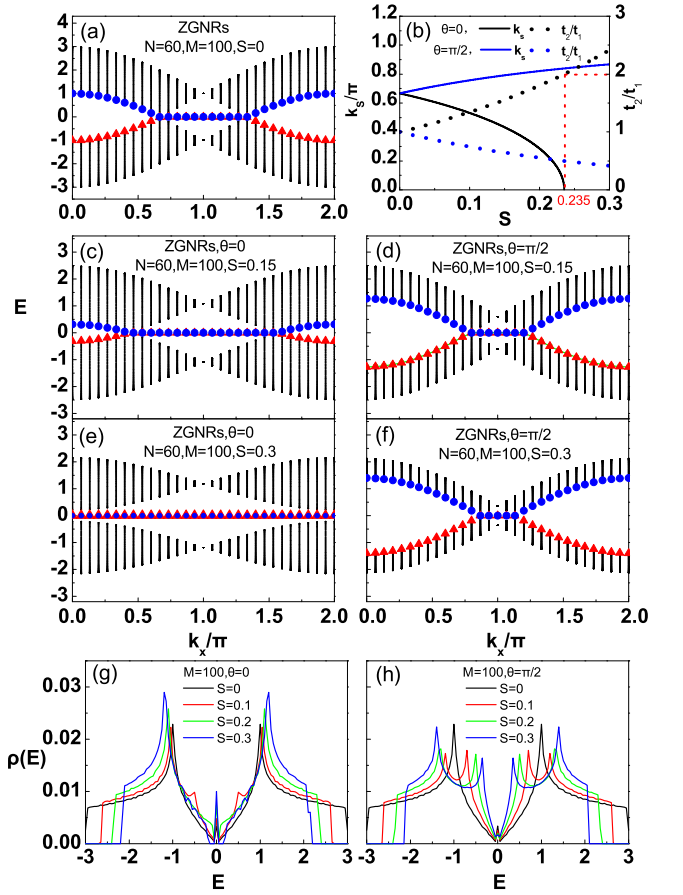


FIG. 4: (Color online.) Band structures of ZGNRs with $N = 60$ and $M = 100$ for various sizes and strains in (a) and (c)-(f). (g) and (h) are the density of states $\rho(E)$ of strained ZGNRs with $M = 100$ and $N = 1600$ for $\theta = 0$ and $\theta = \pi/2$, respectively. (b) shows the strain dependence of k_s and t_2/t_1 (see text for details).

with increasing S until $S = S_c$, after that $k_s = 0$ and the flat band with zero energy extends over the whole Brillouin zone accompanied by the conduction and valence bands detached from each other. S_c is the same as that defined for AGNRs in previous subsection which signals the dimerization of the t_2 -bonds. In contrast, for the vertical strain of $\theta = \pi/2$, k_s moves toward π with increasing S and the flat band shrinks into a single point with $k_s = \pi$ in the large S limit as shown in Figs. 4(d) and (f).

In fact, the range of the momentum for the flat band is given by the convergent condition on the wave function, which requests $|2t_1/t_2 \cos(k_x/2)| \leq 1$ leading to $k_s = 2\cos^{-1}(t_2/2t_1)$ [13]. We plot k_s and t_2/t_1 as functions of strain S in Fig. 4(b). When $\theta = 0$, $t_2/(2t_1) \leq 1$ holds only for $S \leq S_c = 0.235$, where k_s has a solution between 0 and π . If $S > S_c$, $t_2/(2t_1) > 1$ and the convergent condition holds for all possible momentum k_x , therefore the flat band extends throughout the whole Brillouin zone. When $\theta = \pi/2$, $t_2/(2t_1) \leq 1$ is satisfied

for any positive S . In this case, k_s always has a solution between 0 and π . We note that the flat band can shrink into a point with $k_s = \pi$ if $t_2 = 0$, which corresponds to the horizontal t_2 -bonds broken and the ribbon becomes M independent carbon chains connecting the left and right electrodes.

The edge states are also revealed by the zero energy peak in the DOS shown in Figs. 4(g) and (h). As the tensile strain increases, the peak intensity is enhanced for $\theta = 0$, while it is suppressed for $\theta = \pi/2$. This coincides with previous analysis for the region of momentum allowed for the edge states. Similar to the AGNRs, the band width is $D = 2t_1 + t_2$ with a minor correction proportional to M^{-1} , which also shrinks with increasing S . In fact, except for the additional zero energy peaks, the characteristics of $\rho(E)$ for ZGNRs under the uniaxial strains with $\theta = 0$ (or $\theta = \pi/2$) are quite similar to those for AGNRs with $\theta = \pi/2$ (or $\theta = 0$), including the positions of the shoulders for $S = 0.1$ and of double peaks, since the lattice coordinates of ZGNRs can be obtained from that of AGNRs rotated by $\pi/2$.

IV. TRANSPORT PROPERTIES OF GRAPHENE NANORIBBONS

The interplay between the strain and the finite size effect leads to the fine tuning of the band structures of GNRs as presented in the previous section. This allows GNRs to be considered as a promising candidate for mechanically controllable electronic nano-devices. In this section, we use the transfer matrix method described in Sec. II B to explore in details the transport properties of strained GNRs with various sizes and gate voltages as well. The transport properties essentially depend on both the band structures of GNRs and two leads. Transport results discussed in this section are expected to bring some insights into the designation of GNR-based nano-devices for experimentalists.

A. Conductance of strained AGNRs

We first discuss the conductance G of neutral GNRs, i.e., the gate voltage $V_g = 0$. As discussed in Sec. III A, the band gaps oscillate with the strains and ribbon widths, which signals one sort of the metal-semiconductor transition[16, 18]. This results in that the conductances in Fig. 5 also oscillate accordingly, where the conductance peaks are precisely located at the gapless points of Fig. 3.

Figures 5(a) and (b) show the conductances for the narrow ribbons with $M \leq N$. When M is small enough, say $M = 10$, all the maxima of G equal $2e^2/h$, which implies that only one effective conducting channel is maximally opened due to the strong confinement in the y direction. As the ribbon width increases from 10 to 400 as shown in Figs. 5(a-d), more and more channels are

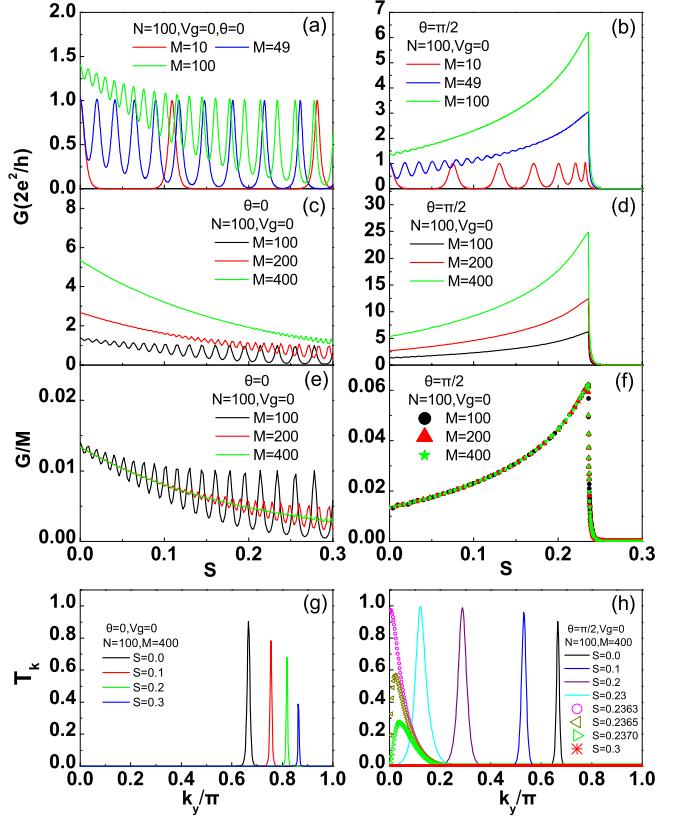


FIG. 5: (Color online.) The strain dependence of the conductance in charge neutral AGNRs (i.e. $E = V_g = 0$) for different ribbon widths M . The tension is along x -axis in (a), (c) and (e), and along y axis in (b), (d) and (f). (e) and (f) show the universal behavior of the scaled conductance G/M with $M \geq N$ particularly. (g) and (h) display the transmission probabilities in different channels for $\theta = 0$ and $\theta = \pi/2$, respectively.

involved in the electronic transport, leading to the enhancement of the conductance. In fact G is almost linear in M for AGNRs with fixed lengths, which is reflected by the universal strain dependence of G/M in Fig. 5(e,f). Besides the ribbon width, the hopping amplitude t_2 also has a positive correlation with the conductance. As one can see in an extreme situation as indicated by the geometry of AGNRs in Fig. 1, that if $t_2 = 0$, the electronic transport would be completely shut down. At the same time t_2 is controlled by the strain, which monotonically decreases for $\theta = 0$ and increases for $\theta = \pi/2$ when S increases as shown in Fig. 2(a). This explains the strikingly different strain dependence of the conductance in Fig. 5(c) for $\theta = 0$ and in Fig. 5(d) for $\theta = \pi/2$ (with $S < S_c$), respectively. Figs. 5(a)-(f) also indicate that the conductance oscillation is greatly suppressed in wider ribbons. For the ribbons with the same size, the oscillation is obviously violently under the horizontal strain than that under the vertical one.

It is interesting to note that when $\theta = \pi/2$, the conductance of AGNRs vanishes completely in the region

$S > S_c$ for any widths. This is because a gap is opened in this region mainly by the uniaxial strain, on which the ribbon width has little effect. In fact there is a quantum phase transition occurring at the critical strain S_c as we have discussed in Sec. III A. Correspondingly, we find a λ -like in the strain dependence of the conductance in Figs. 5(d,f). The sudden drop of the conductance is expected useful in the identification of the tension-driven phase transition, as well as the determination of the critical strain accurately via electronic measurements.

To further understand the electronic transport features of AGNRs, we plot the transmission probability $T_k(k_{y,n}) \equiv \sum_{n'} \eta_{nn'} |t_{nn'}|^2$ [23] under different circumstances as functions of $k_{y,n}$ in Fig. 5(g) for $\theta = 0$ and Fig. 5(h) for $\theta = \pi/2$. One can see then T_k has a spike at the momentum k_s , which is exactly the onset momentum of the flat band in the spectra of ZGNRs with the same strain as seen in Figs. 4. In fact, the interface between each lead and the AGNR has a zigzag pattern, where localized states might exist similar to the edge states in ZGNRs. As long as k_y is close enough to k_s , the localization length is comparable to the ribbon length[29–31]. Therefore the corresponding quantum states extend from the left lead to the right one, giving the major contributions to the conductances. For $\theta = 0$, the peak position k_s moves from $2\pi/3$ towards π and the peak height decreases with increasing S . However, when $\theta = \pi/2$, k_s moves towards zero and the height increases slightly as S increases, until $S = S_c$. After that, the peak position shifts backward and the height drops rapidly when $S > S_c$. For $S = 0$, the analytic T_k obtained in Ref.23 gives rise to $GN/M = 4e^2/3h$ at $V_g = 0$ as $N, M \rightarrow \infty$ and $M/N \gg 1$. This finite value is the maximal value for $\theta = 0$ and all S , but the minimal value for $\theta = \pi/2$ and $S < S_c$.

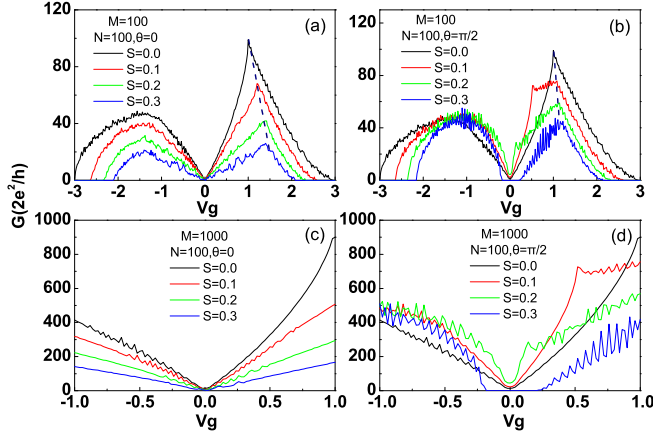


FIG. 6: (Color online.) The conductance of AGNRs as a function of the gate voltage V_g : (a) and (c) for $\theta = 0$, (b) and (d) for $\theta = \pi/2$. The size parameters: (a) and (b) with $N = 100$ and $M = 100$, (c) and (d) with $N = 100$, $M = 1000$.

Figure 6 with $M = N = 100$ shows the overall features of the conductance as a function of the gate volt-

age for AGNRs. One can see that the conductance is not symmetric with respect to $V_g = 0$, revealing an electron-hole asymmetry, which has been observed in many experiments[1–3]. This is a direct consequence of using ordinary metallic leads[23]. It is well-known that a tight binding model on a bipartite lattice with only nearest neighbor hopping is e-h symmetric. In the present system, the interface between each lead and the AGNR consists of five-atom rings, which cannot be bipartite and breaks the e-h symmetry eventually[30]. One can also see that the conductance fluctuates with V_g , which is due to the scattering of electrons off the lead-ribbon interfaces and the armchair edges, since there is no impurity and disorder in the present system. The edges reflection of AGNRs can be suppressed relatively by increasing the width as demonstrated in Figs. 6(c) and (d) with $M = 1000$, especially for small gate voltage and strains. The remaining fluctuations in Figs. 6(c,d) should be attributed essentially to the scattering on the lead-ribbon interfaces.

In Fig. 6(a) for $\theta = 0$, the conductance curves are rather smooth for $V_g < 0$ and show a cusp at $V_g = 2t_1 - t_2 > 0$ corresponding to the higher energy peak of $\rho(E)$ in Fig. 2(g) and moves outwards as S increases. However, the lower energy peak of $\rho(E)$ at $E = t_2$ shows no evidence in the conductance curves. When $\theta = 0$, the conductances are suppressed by increasing S for all V_g as observed in previous studies[9, 10]. As a contrast, when $\theta = \pi/2$, the conductance in Fig. 6(b) shows a more complicated V_g -dependence, which reflects the significant differences between the strain dependences of the band structures in the two cases. When S increases but is still smaller than S_c , we find the conductance dome in the negative energy region, an abrupt increase for $0 < V_g < 2t_1 - t_2$, a gentle slop for $2t_1 - t_2 < V_g < t_2$, and finally a decreasing region for $V_g > t_2$. Although the hopping amplitudes t_i 's shift with S , we can still claim that, G is an increasing function of S for small V_g , and a decreasing function for large V_g . When $S \geq S_c$, a gap Δ opens and G vanishes for $V_g < \Delta$ and is suppressed by increasing S for any $V_g > \Delta$ as can be seen in Figs. 6(b) and (d).

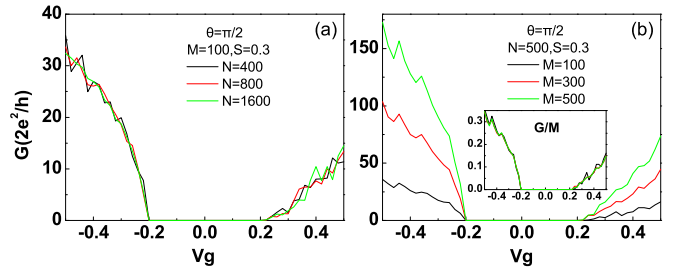


FIG. 7: (Color online.) The conductance of AGNRs for the vertical strain $S = 0.3 > S_c$ with various lengths N and widths M . Inset in (b): the conductance scaled by the width M .

Figures 7(a) and (b) show more details on G for $S =$

0.3 and $-0.5t_0 < V_g < 0.5t_0$. The conductance is zero for $-0.2t_0 < V_g < 0.2t_0$, which indicates $\Delta = 0.4t_0$ for $S = 0.3$ in consistency with that from the direct calculation given in Fig. 3(e). Fig. 7(a) also implies that as $N \geq 400$ the conductance barely changes with increasing N due to the ballistic transport. Fig. 7(b) shows the dependence of the conductance on M and its inset reveals the universal behavior of renormalized conductance G/M .

B. Conductance of strained ZGNRs

Figures 8(a)-(d) display the conductance of the ZGNRs as a function of V_g with various S and M for fixed $N = 100$. In particular, Figs. 8(a) and (b) with $M = 101$ show the overall features of G in the full range of the band width, while Figs. 8(c) and (d) with a larger $M = 901$ is shown to demonstrate less conductance fluctuations for $|V_g| \leq 1.0$. The conductance data obviously shows the e-h symmetry unlike the AGNRs case. This is because the whole system is still bipartite since those rings on the interfaces between the leads and ZGNR contain either four or six atoms as seen in Fig. 1(b), in contrast to the non-bipartite five-atom rings on the interfaces in the system of AGNRs. It thus seems that all the features of the conductance are essentially consistent with the DOS for ZGNRs in Fig. 4. It is also remarkable that the conductance is a constant around G_0 ($G_0 \equiv 2e^2/h$) or vanishingly small at zero gate voltage in the large N and M limit and the flat band is apparently not involved in electronic transport even at $V_g = 0$. This feature is unchanged under the strains and we will discuss it latter.

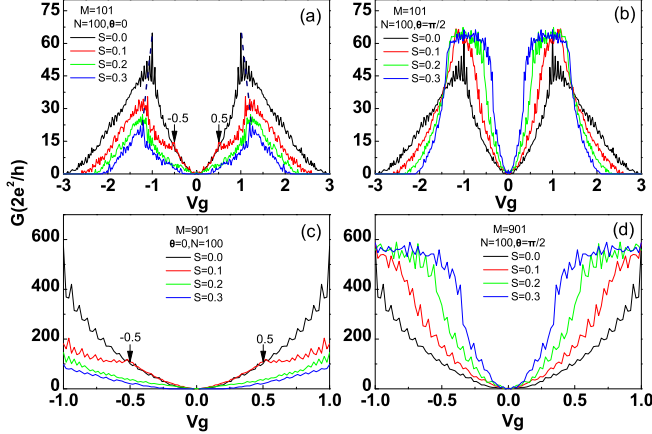


FIG. 8: (Color online.) The conductance of ZGNRs as a function of the gate voltage V_g : (a) and (c) for $\theta = 0$; (b) and (d) for $\theta = \pi/2$. The size parameters: (a) and (b) for $N = 100$ and $M = 101$; (c) and (d) for $N = 100$ and $M = 901$.

In Fig. 8(a) for $\theta = 0$, two sharp peaks of the conductance for each different strain correspond to the peaks of $\rho(E)$ at $E = \pm t_2$ in Fig. 4(g), which move outwards when the strain increases. It is interesting to note that in Figs. 8(a) and (c) the conductance for $S = 0.1$ is almost

identical to that for $S = 0$ in the region $|V_g| < 0.5t_0$. In fact this phenomena emerges for any given strain $S < S_c = 0.235$, and the overlapping region between $G(S)$ and $G(0)$ is given by $|V_g| < 2t_1 - t_2$ which is obviously strain dependent. In other word, given a small V_g , the relation $|V_g| = 2t_1 - t_2$ gives rise to a threshold of strain, below which the measured conductance barely changes with respect to S . Despite of this identical region, Fig. 8(a) for $\theta = 0$ also indicates that the conductance is reduced with increasing S if the gate voltage is fixed. Figs. 8(b) and (d) show the conductance for $\theta = \pi/2$, where we find a cross point of the conductance curves under different strains. For convenience we denote the corresponding gate voltage as V_g^C which is around $1.5t_0$. The strain enhances the conductance for $|V_g| < V_g^C$ and suppresses it otherwise.

To interpret the difference of the conductances between $\theta = 0$ and $\theta = \pi/2$, we recall that the hopping integrals t_i 's have different strain dependence as seen in Fig. 2(a). When the strain increases for $\theta = 0$, t_2 increases, while $t_{1,3}$ decreases. However, $t_{1,3}$ effectively favors the horizontal electronic transport, while t_2 may cause the formation of the dimers for vertical bonds which hinders the electrons from moving freely. Therefore, the conductance is reduced by increasing the strain for given V_g . However, for $\theta = \pi/2$, both $t_{1,3}$ and t_2 decrease, but t_2 drops faster. As a consequence, the ribbon tends to form M metallic chains with a weak interchain coupling. The conductance is then enhanced with an upper limit MG_0 as $t_2 \rightarrow 0$ for small V_g . Since more and more channels below V_g^C are fully filled due to the reduction of the hopping amplitudes $t_{1,3}$, they do not contribute to the conductance for large gate voltage. It turns out that there are two turning points $\pm V_g^C$ in Fig. 8(b) and opposite strain dependences of the conductance are found for $|V_g| < V_g^C$ and for $|V_g| > V_g^C$, respectively.

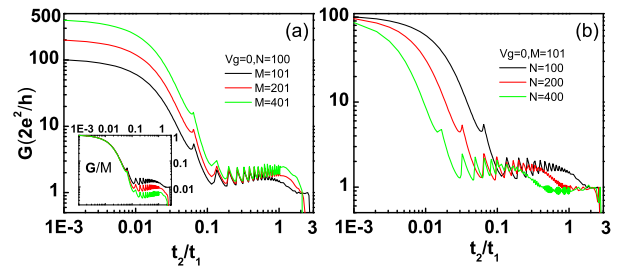


FIG. 9: (Color online.) The conductance versus t_2/t_1 at $V_g = 0$ with $t_1 = 0.96$ fixed. (a) for $N = 100$ and $M = 101, 201$ and 401 ; and (b) for $M = 101$ and $N = 100, 200$ and 400 . Inset in (a) for the conductance scaled by the width M .

For ZGNRs, the topology of structure not only protect the e-h symmetry of the electronic transport but also stimulates the analysis of more general features of the conductance in a whole range of t_2/t_1 , which might be beyond the values given by the relations Eqs. (3). In principle, one has actually two limits: $t_2/t_1 \gg 1$ and $t_2/t_1 \ll 1$. For the former case, the system possesses an

ordered and insulating ground state consisting of dimerized t_2 -bonds, which already emerges actually with a zero conductance at $t_2/t_1 \approx 2.9$ for $M = 101$ and $N \gtrsim M$ as demonstrated in Fig. 9(a) and (b). When $t_2/t_1 \ll 1$, the honeycomb lattice becomes M weakly coupled metallic (zigzag) chains and the conductance reaches its maximal value MG_0 as seen in Fig. 9(a) where the conductance is shown as a function of t_2/t_1 for $N = 100$ with $M = 101, 201$ and 401 . One can see that G is enhanced by decreasing t_2/t_1 and indeed proportional to M as being well renormalized by M for $t_2/t_1 \lesssim 0.05$ in the inset. Fig. 9(b) shows that the conductance is also reduced by increasing the length of ribbons, implying a non-ballistic transport. In addition, the conductance fluctuations around G_0 show up for $t_2/t_1 \gtrsim 0.1$.

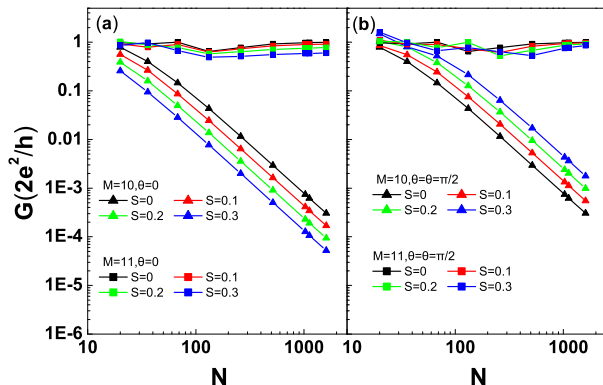


FIG. 10: (Color online.) Odd-even M effects on the conductance for narrow ZGNRs for $\theta = 0$ in (a) and $\theta = \pi/2$ in (b).

Figure 10 shows an even-odd M effect on G for ZGNRs, which is relevant for either experiments or designing nano-devices with narrow and short ribbons. This effect diminishes for sufficiently wide and long ribbons so that our above discussions for Figs. 8 and 9 are given just for odd but sufficiently large M . For $S = 0$ and $V_g = 0$, one finds that the conductance of narrow ZGNRs shows two different scaling behaviors according to the parity of M as $N \rightarrow \infty$ [32, 33]. The conductance is a constant around G_0 for odd M to indicate metallic nature, while $G \sim N^{-2}$ for even M to present a semiconducting feature [30]. In the presence of strains, one can still find two types of scaling behaviors for the conductance at $V_g = 0$ as shown in Figs. 10(a) and (b). When M is odd, the conductance changes a little with both N and S . When M is even, although the conductance decreases in a power law N^{-2} , G is suppressed for $\theta = 0$ and enhanced for $\theta = \pi/2$ with increasing S if N is fixed.

V. EFFECTS OF EDGE RELAXATION

In realistic situations, there may exist passivation and spin polarization on the ribbon edges, which affect the band structure of narrow ribbons [28]. However, these

edge modes only affect the edge and nearby carbon atoms for wide enough ribbons, in contrast, the strain can affect all the carbon-carbon bonds in the ribbon. As shown in Fig. 3, the band gaps oscillate with the strain for all types of AGNRs and is around $0.25t_0$ for $M = 10$ (i.e., $N_a = 20$), while the edge relaxation induces one only around $0.032t_0$ as shown in Ref. 28. This indicates the edge relaxation has much smaller effect on the band gap than the strain effect, which even becomes smaller and smaller as the ribbon width increases.

Comparing with the strain effect, edge relaxation on the transport properties of GNRs is negligible in relatively wide graphene ribbons. In Fig. 11, the black solid lines are the conductance of pristine GNRs and the others are the data with edge relaxation. For AGNRs, we set the hopping integral at the edge t_e to be $1.12t_0$ as suggested in Ref. 28 and the on-site energies ϵ_{0e} being $0.1t_0$ and $0.2t_0$. It is clearly seen that the effects of edge relaxations on electronic transport are negligible as anticipated for armchair ribbons wider than 10nm (i.e., $M \geq 42$). For ZGNRs, it is well known that tight binding parameters of carbon atoms based on first-principle calculation are environment dependent, such as QUAMBOs tight binding (QUAMBOs-TB) parameters as shown in [34]. We set the hopping integral at the edge $t_e = 1.05t_0$ and the on-site energies ϵ_{0e} being $0.25t_0$ according to [34]. It is clearly seen that the effects of edge relaxations on electronic transport are negligible for zigzag ribbons wider than 10nm (i.e., $M \geq 48$).

In simple tight binding model, edge spin polarized states of ZGNRs requires the introduction of Coulomb interaction into the flat band. However, these magnetic moments at the edges of zigzag nanoribbons (for correlation effects) are far beyond the scope of the present investigation. Similar to edge relaxation, edge spin polarization only affects the edge atoms and these spin polarized edge modes can provide at most two conducting channels. Therefore, their effect on the electronic transport is expected to be less important than the strain effect which is on all the bulk conducting channels. As a consequence, when investigating the strain effect on the transport through GNRs, one can ignore these edge effects.

VI. SUMMARY AND CONCLUSIONS

In this article, we have investigated the electronic transport of graphene nanoribbons under various tensile strains with connections to the normal metallic leads. For this purpose, we first calculated the band structures of strained GNRs with both zigzag and armchair edges. The direction of the uniaxial tension, which is taken to be either parallel ($\theta = 0$) or perpendicular ($\theta = \pi/2$) to the ribbon axis, has a crucial effect on the band structure.

In the strained armchair GNRs with $\theta = 0$, the band gap oscillates with the strain in a zigzag pattern, leading to the transitions between metal and semiconductor. The

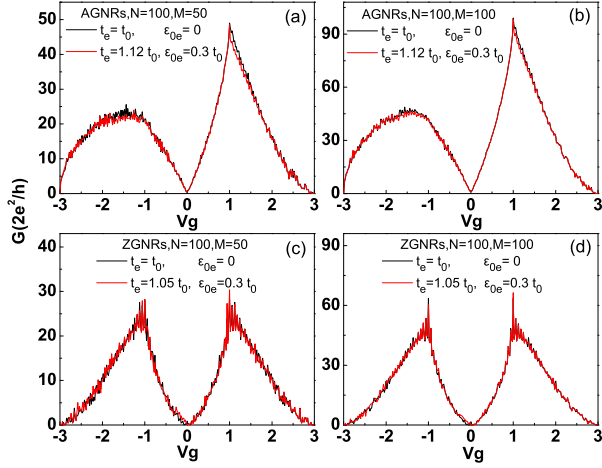


FIG. 11: (Color online.) Effects of edge relaxation on the conductance of AGNRs (a,b) and ZGNRs (c,d) with various sizes.

oscillatory amplitude is almost unchanged as S increases. This kind of band gap is mainly a finite width effect, since it vanishes as M goes to infinity. If $\theta = \pi/2$, similar oscillatory gap also appears, but only for the strains smaller than a critical value S_c . As S approaches S_c , the oscillatory amplitude goes to zero, unlike the case for $\theta = 0$. Once $S > S_c$, the other kind of band gap opens which is linear in $S - S_c$ and hardly affected by the ribbon width. In fact as the strain with $\theta = \pi/2$ increases, a quantum phase transition is induced at $S = S_c$ to separate a liquid phase from a solid phase where the bonds perpendicular to the strain are dimerized.

In the zigzag GNRs, the most intriguing phenomenon is the appearance of the flat band in a region of momentum $[k_s, 2\pi - k_s]$. As the strain with $\theta = 0$ increases, k_s decreases to zero until $S = S_c$, then the flat band extends throughout the full Brillouin zone, and the conduction and valence bands are separated. On the contrary, with increasing S , k_s moves towards π and the region of the

flat band shrinks into a point for $\theta = \pi/2$.

Except for the flat band, most features on the strain-dependence of the band structures are well revealed by the behaviors of the conductance of GNRs. For example, the band gap oscillation results in the conductance oscillation at the zero gate voltage $V_g = 0$ as the strain varies. The peak in the plot of the conductance versus V_g is compatible with that in the DOS plot. Note that not all the modes with energy V_g contribute to the conductance, but only those satisfying the boundary conditions are responsible for the electronic transport, therefore, it is not necessary to have a one-to-one correspondence between the peaks of the conductance and those of the DOS. Furthermore, by measuring the strain dependence of the conductance of AGNRs at $V_g = 0$, one can also detect the quantum phase transition induced by the tension perpendicular to a C-C bond and determine the critical strain as well.

Since we connect the GNRs with square lattices as the metallic electrodes, it is worth mentioning the fundamental effect of the topology of the heterojunctions on the conductance of GNRs. In particular, due to the non-bipartite feature of the electrode-AGNR interfaces, the conductance data of AGNRs is not e-h symmetric, while this kind of symmetry can still be found in that of ZGNRs, since the electrode-ZGNR interfaces do not break the bipartite structure of the whole system. This phenomenon has no counterpart in the band structures obtained with periodic boundary condition, yet it may be important for designing the nano-size devices.

VII. ACKNOWLEDGEMENTS

This work is supported by the National Basic Research Program of China (2012CB921704) and NSF of China (Grant Nos. 11174363, 11204372, 11374135). We thank G.H. Ding for helpful discussions.

-
- [1] K. S. Novoselov, A. K. Geim, S. V. Morozov, D. Jiang, M. I. Katsnelson, I. V. Grigorieva, S. V. Dubonos, and A. A. Firsov, *Nature (London)* 438, 197 (2005).
 - [2] K. S. Novoselov, A. K. Geim, S. V. Morozov, D. Jiang, Y. Zhang, S. V. Dubonos, I. V. Grigorieva, and A. A. Firsov, *Science* 306, 666 (2004).
 - [3] F. Miao, S. Wijeratne, Y. Zhang, U. C. Coskun, W. Bao, and C. N. Lau, *Science* 317, 1530 (2007).
 - [4] V. M. Pereira and A. H. Castro Neto, *Phys. Rev. Lett.* 103, 046801 (2009).
 - [5] K. S. Kim, Y. Zhao, H. Jang, S. Y. Lee, J. M. Kim, K. S. Kim, J. H. Ahn, P. Kim, J. Y. Choi, and B. H. Hong, *Nature* 457, 706 (2009).
 - [6] T. M. G. Mohiuddin, A. Lombardo, R. R. Nair, A. Bonetti, G. Savini, R. Jalil, N. Bonini, D. M. Basko, C. Galiotis, N. Marzari, K. S. Novoselov, A. K. Geim, and A. C. Ferrari, *Phys. Rev. B* 79, 205433 (2009).
 - [7] C. G. Lee, X. D. Wei, J. W. Kysar, and J. Hone, *Science* 321, 385 (2008).
 - [8] E. Cadelano, P. L. Palla, S. Giordano, and L. Colombo, *Phys. Rev. Lett.* 102, 235502 (2009).
 - [9] X. W. Fu, Z. M. Liao, J. X. Zhou, Y. B. Zhou, H. C. Wu, R. Zhang, G. Y. Jing, J. Xu, X. S. Wu, W. L. Guo, and D. P. Yu, *Appl. Phys. Lett.* 99, 213107 (2011).
 - [10] S. H. Bae, Y. Lee, B. K. Sharma, H. J. Lee, J. H. Kim, J. H. Ahn, *Carbon* 51, 236 (2013).
 - [11] Y. Wang, R. Yang, Z. Shi, L. Zhang, D. Shi, E. Wang, G. Zhang, *ACS Nano* 5, 3645 (2011).
 - [12] V. M. Pereira, A. H. Castro Neto, and N. M. R. Peres, *Phys. Rev. B* 80, 045401 (2009).
 - [13] Y. Li, X. W. Jiang, Z. F. Liu, and Z. R. Liu, *Nano Res.* 3, 545 (2010).

- [14] X. Peng, F. Tang, and A. Copple, J. Phys.: Condens. Matter 24, 075501 (2012).
- [15] Y. Lu and J. Guo, Nano Res. 3, 189 (2010).
- [16] M. Poetschke, C. G. Rocha, L. E. F. F. Torres, S. Roche, and G. Cuniberti, Phys Rev B 81, 193404 (2010).
- [17] J. Y. Wang, Z. F. Liu, and Z. R. Liu, AIP Advances 2, 012103 (2012).
- [18] R. Rasuli, H. Rafii-Tabar, and A. I. Zad, Phys Rev B 81, 125409 (2010).
- [19] Zenan Qi, D. A. Bahamon, Vitor M. Pereira, Harold S. Park, and D. K. Campbell, Nano Lett. 13, 2692-2697 (2013)
- [20] T. Low and F. Guinea, Nano Lett. 10, 3551 (2010).
- [21] H. Rostami and R. Asgari, Phys. Rev. B, 88, 035404 (2013).
- [22] D. A. Bahamon and V. M. Pereira, Phys. Phys. Rev. B 88, 195416 (2013).
- [23] S. J. Hu, W. Du, G. P. Zhang, M. Gao, Z. Y. Lu and X. Q. Wang, Chin. Phys. Lett. 29, 057201 (2012).
- [24] O. L. Blakslee, D. G. Proctor, E. J. Seldin, G. B. Spence, and T. Weng, J. Appl. Phys. 41, 3373 (1970); D. Portal, E. Artacho, J. M. Soler, A. Rubio, and P. Ordejon, Phys. Rev. B 59, 12678 (1999).
- [25] Y. Yin, S. J. Xiong, Phys. Lett. A 317, 507 (2003).
- [26] M. Gao, G. P. Zhang, Z. Y. Lu, Comput. Phys. Commun. 185, 856 (2014).
- [27] Y. X. Yao, C. Z. Wang, G. P. Zhang, M. Ji and K. M. Ho, J. Phys.: Condens. Matter 21, 235501 (2009).
- [28] Y. W. Son, M. L. Cohen and S. G. Louie, Phys. Rev. Lett. 97, 216803 (2006). Note that N_a in their paper equals to $2M$, therefore the gapless condition $\bmod (N_a, 3) = 2$ in their paper for unstrained AGNRs is the same as ours $\bmod (M, 3) = 1$ given in Sec. III A.
- [29] K. Nakada, M. Fujita, G. Dresselhaus, and M. S. Dresselhaus, Phys. Rev. B 54, 17954 (1996).
- [30] G. P. Zhang and Z. J. Qin, Chem. Phys. Lett. 516, 225 (2011).
- [31] Katsunori Wakabayashi, Mitsutaka Fujita, Hiroshi Ajiki, Manfred Sigrist, Phys. Rev. B 59, 8271 (1999).
- [32] G. P. Zhang and Z. J. Qin, Phys. Lett. A 374, 4140 (2010).
- [33] Z. Y. Li, H. Y. Qian, J. Wu, B. L. Gu and W. H. Duan, Phys. Rev. Lett. 100 (2008) 206802.
- [34] Fang X W, Zhang G P, Yao Y X, Wang C Z, Ding Z J and Ho K M 2011 Phys. Lett. A 375, 3710